Implementation of the Hess–Smith and Weissinger methods

Diogo Martins[1], Gabriele Pagnoni[2], Riccardo Rossetti[3], Tommaso Rossi[4], Lorenzo Rota[5]

[1]diogo.rebelo@mail.polimi.it & 301549
[2]gabriele.pagnoni@mail.polimi.it & 299997
[3]riccardo2.rossetti@mail.polimi.it & 301315
[4]tommaso9.rossi@mail.polimi.it & 299222
[5]lorenzo5.rota@mail.polimi.it & 299534

24 December 2025

1. Hess-Smith method implementation and validation

To evaluate the implementation of the Hess-Smith method on the NACA 0008, we computed the C_p distribution, C_l, and C_m for $\alpha = 1°$ and $\alpha = 2°$, and then validated the results using XFOIL. Examining the C_p plot (Figure 1), it can be seen that there are no significant differences. The nearly identical C_l values further confirm this.

However, the C_m are significantly different (-0.0008 in XFOIL vs -0.0016 in Hess-Smith at $\alpha = 1°$). A closer inspection of the C_p plot reveals that the largest differences occur near the trailing edge, which, having a larger moment arm relative to the aerodynamic center, strongly influence the moment coefficient. The difference is more pronounced in this region because the NACA 0008 is thin and has a sharp trailing edge, which makes paneling more challenging and can lead to discrepancies.

To ensure that the observed differences in C_m were solely due to the different numerical approaches, we also analyzed the NACA 0012, a thicker airfoil with a less sharp trailing edge. As expected, the C_m values are similar between the two methods, just like the C_l.

Regarding the applicability limits of this comparison: low angles of attack, to avoid thick boundary layers or flow separation, and low Mach numbers, up to approximately 0.3, where we verified the validity of the results by comparison with XFOIL.

2. Comparison between NACA 0008 and NACA 6412

The NACA 6412 features a pronounced camber (maximum camber of 6%), whereas the NACA 0008 is a symmetric airfoil. Additionally, the NACA 6412 is thicker than the NACA 0008, with a maximum thickness of 12% compared to 8%. These substantial design variations result in quite different aerodynamic responses.

To investigate these different behaviors, the study evaluated different small angles of attack (from 1° to 4°) with two Reynolds numbers ($Re = 10^6$ and $Re = 6 \cdot 10^6$) and three turbulence levels ($N = 6, 9, 12$). All the angles of attack were chosen to be positive.

The NACA 6412 is specifically designed to achieve high C_l combined with moderate C_d, resulting in a high lift-to-drag ratio. This can be understood by examining Figure 3.

The analysis further examined the differences in turbulent transition and flow separation. Due to its significant camber near the leading edge, the NACA 6412 exhibits a C_p

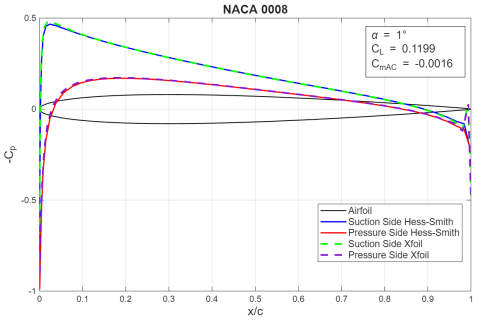

FIGURE 1. -Cp distribution obtained using Hess-Smith and XFOIL

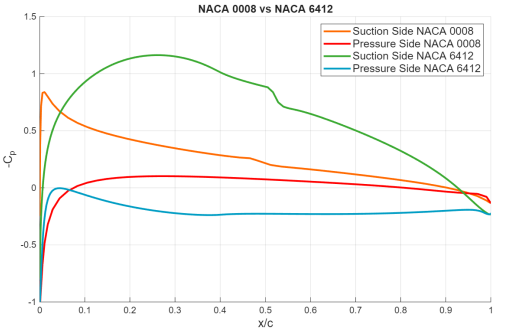

FIGURE 2. Comparison for $Re = 10^6$, $N = 9$, and $\alpha = 2°$

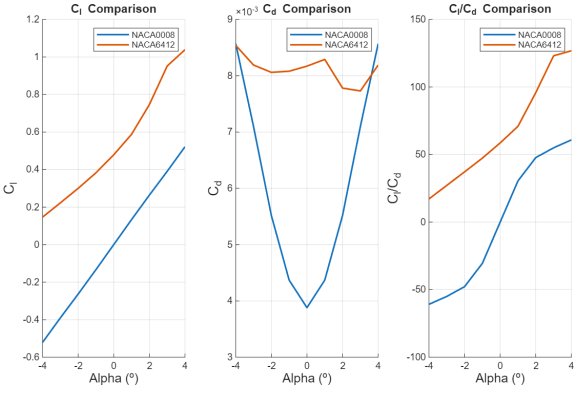

FIGURE 3. Comparison between the C_l, C_d and $\frac{C_l}{C_d}$

Alpha	$\alpha = 1°$	$\alpha = 2°$	$\alpha = 3°$	$\alpha = 4°$
NACA 0008 Top	0.6824	0.4462	0.1901	0.0590
NACA 6412 Top	0.5467	0.5088	0.4918	0.4687

TABLE 1. Transition points for the pressure side of each airfoil for Re = 10^6 and N = 9

distribution on the suction side that is smoother and more rounded compared to the NACA 0008.

As shown in Figure 2, the NACA 6412 experiences a more gradual pressure increase on the suction side (which is the most important for the C_l) than the symmetric profile. Regarding the pressure side, both airfoils show a smooth distribution, although the NACA 6412 maintains higher pressure levels than the NACA 0008.

In the case of the NACA 0008, the suction peak of the pressure coefficient occurs very close to the leading edge, while the subsequent pressure recovery is relatively gradual. This behavior prevents early flow separation, allowing the boundary layer to undergo transition to turbulence beforehand. This mechanism does not occur for the NACA 6412 airfoil. Due to the smoother pressure rise near the leading edge, the pressure recovery must necessarily take place over a shorter chordwise extent. As a result, despite the camber not being excessively high, flow separation occurs before the onset of turbulence.

We can now analyze the effects of varying the angle of attack in terms of turbulence onset and flow separation. The overall shape of the pressure coefficient distribution does

not change significantly by increasing the angle of attack. In both cases, the suction peak moves towards the leading edge and the C_p distribution becomes less smooth.

As indicated in Table 1, the transition point moves more rapidly towards the leading edge on the NACA 0008 airfoil. Considering that increasing the angle of attack increases the probability of flow detachment, because the operating condition moves further away from the Theodorsen angle ($-1.6°$ for the NACA 6412 and $0°$ for the symmetric NACA 0008). In this context, the earlier transition from laminar to turbulent flow on the upper surface of the NACA 0008 effectively prevents separation. On the contrary, transition is not inherently promoted by the geometry of the NACA 6412, leading to phenomena such as laminar separation followed by turbulent reattachment (laminar separation bubble).

Furthermore, it is observed that under certain conditions the NACA 0008 may experience separation prior to transition; however, this separation remains localized due to immediate turbulent reattachment.

Despite these considerations, the NACA 6412 remains a significantly superior airfoil compared to the NACA 0008 for two main reasons. The first is performance-related: although separation is certainly more extensive, the NACA 6412 maintains a considerably higher lift-to-drag ratio due to its much higher C_l. The second reason concerns the structural and geometric characteristics of the two airfoils. The NACA 0008 is very thin and exhibits a sharp curvature near the leading edge. Therefore, at increasing α it becomes comparable to a flat plate. This results in a higher risk of stall at relatively low α (between $7°$ and $10°$, depending on the Re) and makes its operation risky even at $3°$ or $4°$. In contrast, due to its smoother curvature, the NACA 6412 does not suffer from these limitations.

Finally, it should also be noted that turbulence can be deliberately induced on the airfoil surface to delay or prevent separation, which could effectively mitigate potential separation issues on the NACA 6412.

Considering now the effect of turbulence level, represented by the N factor, both airfoils are affected similarly: lower environmental turbulence (corresponding to higher N values) delays the transition to turbulence. The position of the transition point depends on both the airfoil geometry and the specific angle of attack.

Moreover, the N factor influences the separation point: higher N values result in slightly anticipated separation, as the flow remains more laminar and is therefore more prone to detaching. In addition, the drag coefficient C_d increases as N decreases (higher environmental turbulence). Regarding the C_l, only minor variations are observed; it generally increases slightly with higher N values, although this trend is strictly dependent on the presence and extent of flow separation.

3. Weissinger method implementation and validation

The Weissinger method script was validated using XFRL5, a software tool for 3D wing analysis. By using the geometrical data of the planes from task 4, with symmetric NACA profiles for both the wing and tail to have a flat camber line, an inviscid analysis was performed for a range of angles of attack to directly compare the lift and induced drag coefficients. The comparison revealed excellent consistency in the results.

4. Analysis and comparison of Cessna 172 Skyhawk and Piper PA-28

Figure 4 reveals fundamental differences in how each aircraft generates lift across their wingspan. The Cessna 172 shows a circulation distribution closer to the elliptical wing, particularly over the mid-span regions. This indicates a well-designed wing that

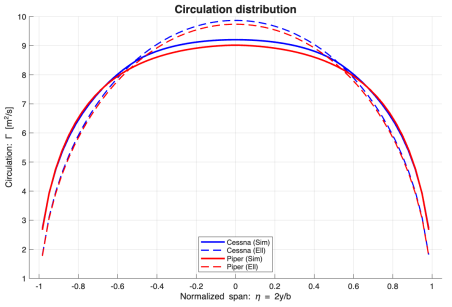

FIGURE 4. Gamma Distribution

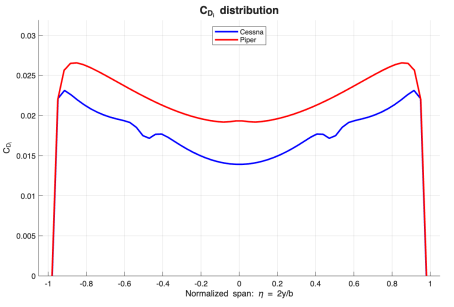

FIGURE 5. C_{di} distribution

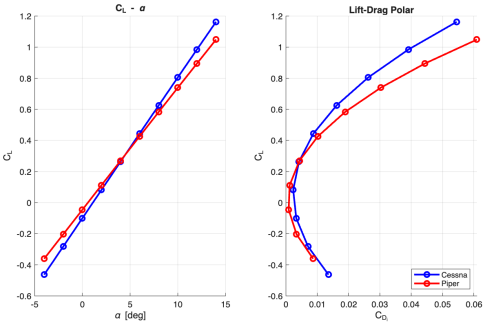

FIGURE 6. Polar

distributes the lift efficiently. The Piper PA-28-180 exhibits lower peak circulation and a deviation from the elliptical distribution; this will also explain the higher induced drag observed in the Piper's polar curve and indicate a less efficient spanwise lift distribution. Therefore, the Cessna 172 has a better lift-to-drag ratio than the Piper PA-28-180.

Figure 5 shows that the Piper's induced drag curve lies above the Cessna's one at the same angle of attack: this confirms the Cessna's wing design superiority in minimizing total induced drag. Furthermore, the Cessna's plot shows two symmetric peaks in local C_d at the normalized span positions $\eta \approx \pm 0.5$, marking the points where the changing of the chord geometry locally perturbs the lift distribution and increases induced drag.

The Piper features a rectangular wing planform: this type of geometry tends to generate lift efficiently at the root but very inefficiently at the tips. The observed "U" shape indicates that the tip vortices are particularly strong, creating a peak in local induced drag. Instead, at the center of the wing, the induced angle of attack is low, creating a minimum. This aligns with the earlier conclusion from the circulation analysis. The Cessna features a semi tapered wing planform: by narrowing the wing towards the tips, the design attempts to recreate the ideal elliptical distribution. Tapering shifts lift inboard, reducing the severity of tip vortices and resulting in a lower medium value for the induced drag curve. The lift curves in Figure 6 for both aircraft show the expected linear relationship at low to moderate angles of attack. However, the Cessna achieves a marginally higher C_L at the same angle of attack. Additionally, for a given C_L, the Piper requires a slightly higher α, implying lower aerodynamic efficiency in lift generation as expected. The polar shows that, particularly at moderate to high C_L's, the Cessna's induced drag coefficient is lower than the Piper's. This is visualized by the Cessna's polar curve lying to the left of the Piper's, confirming the initial observation.